Electronic Supplementary Information

A turn-on fluorescent Zn(II) metal−organic framework sensor for quantitative anthrax biomarker detection

Chao Hong[a,b], *Ling Li**[a] , *Ji-Yong Zou**[a], *Li Zhang*[a] , *Sheng-Yong You*[a]

[a]Institute of Applied Chemistry, Jiangxi Academy of Sciences, Nanchang 330096, PR China

[b]School of Materials Science and Engineering, Nanchang Hangkong University, Nanchang, 330063, PR China

Table S1 Crystal data and Structure Refinements for **1**.

Compound	**1**
Formula	$C_{63.6}H_{41.4}N_3O_{16.2}Zn_3$
formula weight	1302.90
temperature (K)	100.00(10)
crystal system	triclinic
space group	*P*-1
a (Å)	13.1143(3) Å
b (Å)	13.1651(3)
c (Å)	16.3159(4)
α (°)	97.934(2) °
ß(°)	95.154(2) °
γ (°)	92.056(2) °
V (Å^3)	2775.38(11)
Z	2
D_c (g cm^{-3})	1.559
μ (mm^{-1})	1.364
F(000)	1327.0
2θ range (°)	3.122 to 58.936 °
GOF on F^2	1.068
reflections collected / unique	34375 / 12411
R_{int}	0.0284
R_1,[a] wR_2[b] [$I > 2\sigma(I)$]	0.0493, 0.1378
R_1, wR_2 (all data)	0.0706, 0.1497

R_1 [a] = $\sum(|F_0| - |F_c|) / \sum|F_0|$. [b] $wR_2 = [\sum\{w(|F_0|^2 - |F_c|^2)^2\} / \sum[w(|F_0|^2)^2]]^{1/2}$

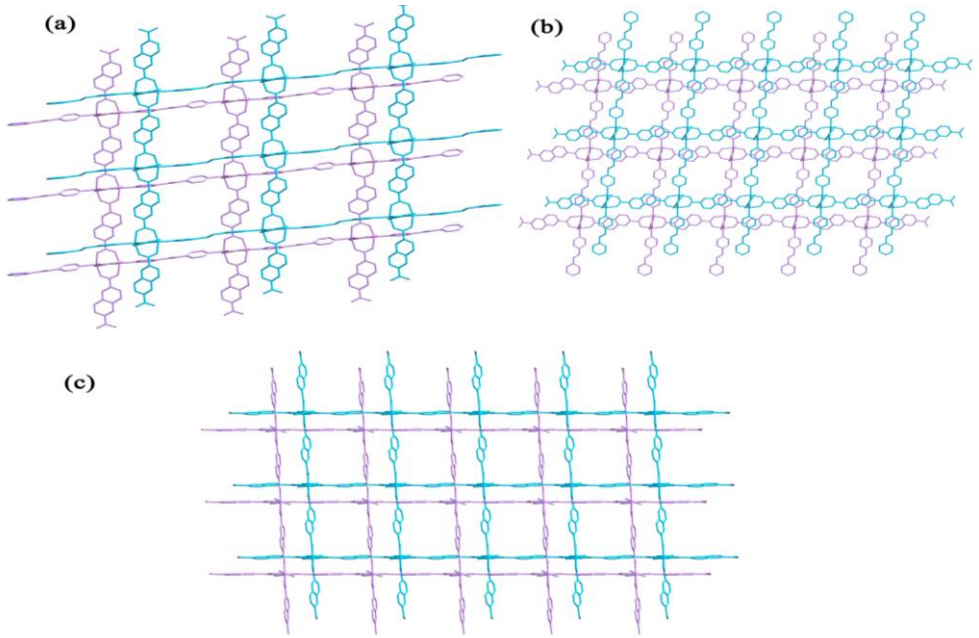

Figure S1 The 3D framework exhibits along the a, b and c directions

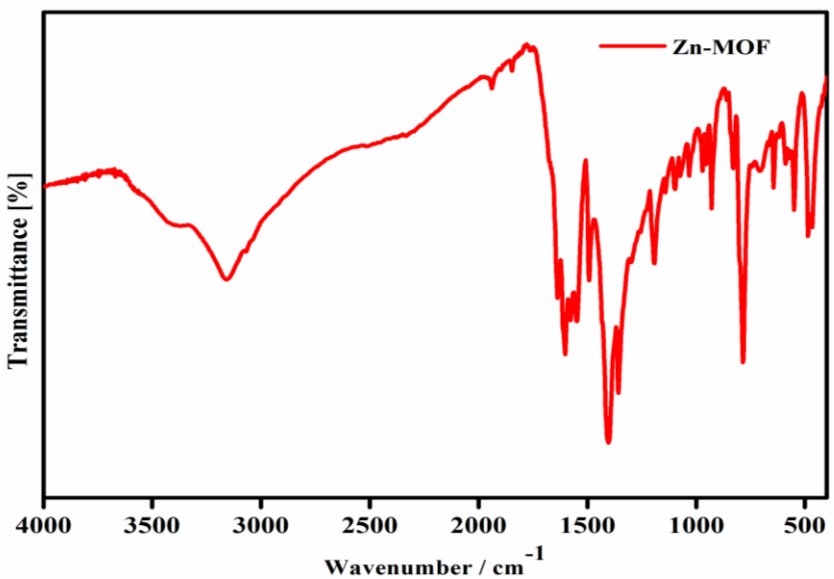

Figure S2 Infrared spectra of **1**.

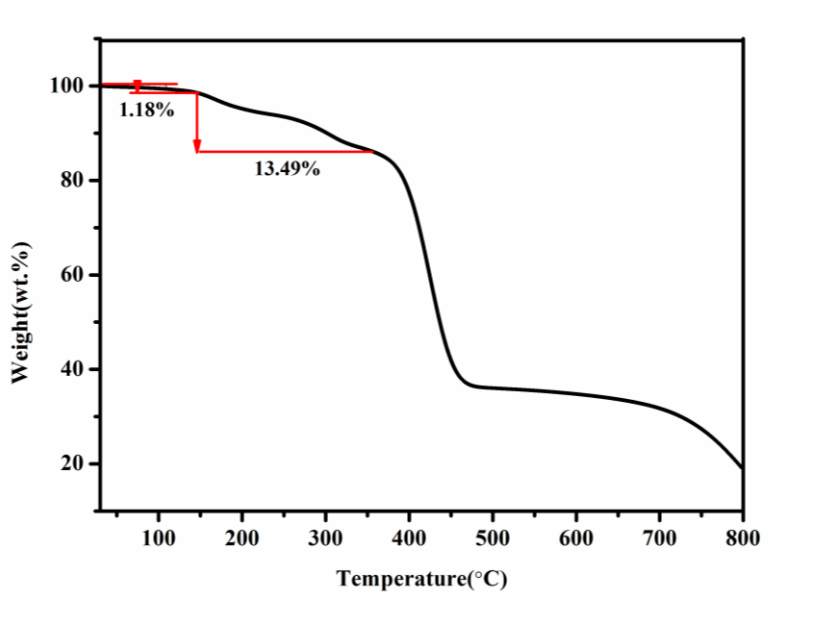

Figure S3 The thermal gravimetric curves (TGA) of **1**.

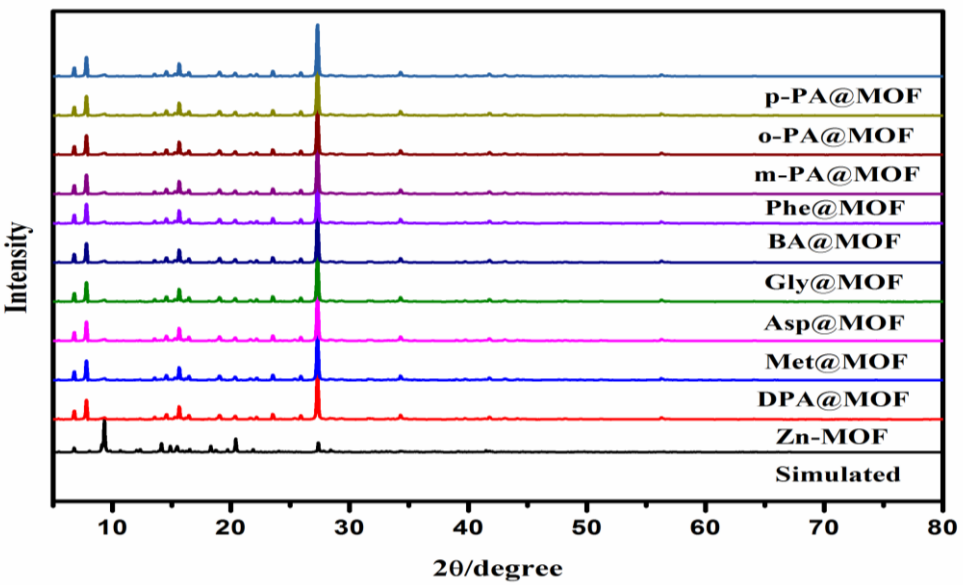

Figure S4 The pxrd contrast diagram of add various interferors and 1

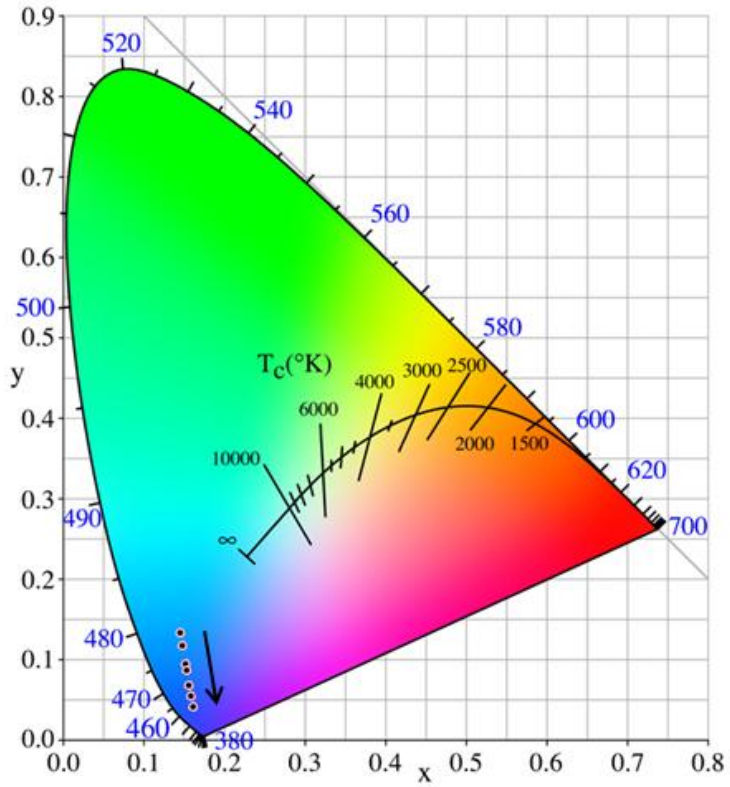

Figure S5 CIE chromaticity diagram showing the color coordinates of **1** and **1** containing DPA**.**

Table S2. Performance comparison of several sensors for the detection of anthrax biomark DPA.

Sensor	Detection mechanism	Detection limit	Reference
1	**turn-on**	**128nM**	**The present work**
Tb-COP	turn-on	13.5 nM	Sens. Actuators, B., 2019, 290, 9
PV-Tb^{3+}	dual colorimetric turn-on	5 μM	Analyst., 2013, 138, 7079
R_6H@Eu(BTC)	dual colorimetric turn-on	4.5 μM	Sens. Actuators, B., 2018, 266, 263
AgNPs−Eu^{3+}	dual colorimetric turn-on	0.31μM	ACS Appl. Nano Mater. 2021, 4, 5469−5477
Eu^{3+}–EBT	dual colorimetric turn-on	2μM	Anal. Chem. 2018, 90, 4221−4225
BCNO QDs-EDTA-Eu^{3+}	Ratiometric fluorescence turn-on	0.5 nM	ACS Appl. Mater. Interfaces 2019, 11, 2336−2343.
TPP/EBT−UCNPs	dual colorimetric turn-on	0.9μM	Anal. Chem. 2019, 91, 18, 12094-12099
R_6G/Eu-CdS@ZIF-8	Ratiometric Fluorescence turn-on	67 nM	Anal. Chem. 2020, 92, 7114−7122.
Tb^{3+}@NH_2- HPU-17	Ratiometric Fluorescence turn-on	44.6 nM	Inorg. Chem. 2021, 60, 2590−2597
Tb-H_2DHBDC	turn-on	2.4 μM	Dalton Trans., 2021, 50, 1300
Eu^{3+}–GMP–Tb^{3+}	dual colorimetric turn-on	96nM	Anal. Chem. 2018, 90, 7004−7011
AuNPs@GSH	dual colorimetric	2 μM	Anal. Bioanal. Chem. 2018, 410, 1805-1815.
CDs-Tb	Ratiometric Fluorescence turn-on	39.4 nM	Nanomaterials 2019, 9, 1234;
$Eu_{0.1}Tb_{0.9}$-BDC	Ratiometric Fluorescence turn-on	2.277μM	J. Mater. Chem. C, 2020, 8, 4392

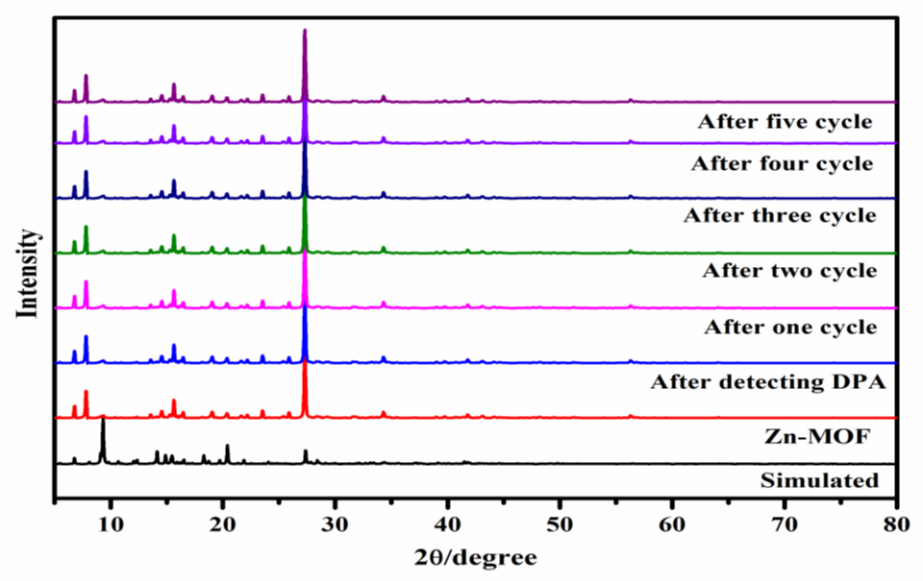

Figure S6 The PXRD patterns of **1** for simulated, as-synthesized and after each recycling experiment of DPA detection

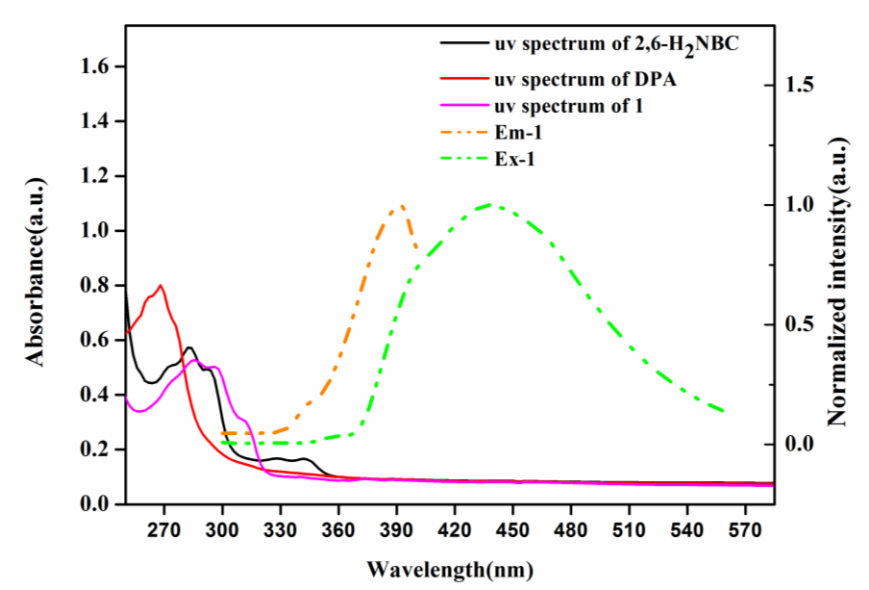

Figure S7 The UV-Vis absorbance spectra of 2.6-H_2NBC ligand, DPA, and **1** and the excitation and emission spectra of **1**

The fluorescence lifetimes of **1** were determined using the following equation based on a bi-exponential fit of the PL decay plots.

$$R(t)=B_1e^{(-t/\tau 1)}+ B_2e^{(-t/\tau 2)}$$

Table S3. Double exponential fitting parameters of PL attenuation graphs doped with DPA of different concentrations

The DPA	τ_1 (ns)	Std. dev.(ns)	τ_2 (ns)	Std. dev.(ns)	X_2
0.00mM	4.6148	0.1104	13.1015	0.2192	1.0483
0.32mM	0.7654	0.0123	3.4624	0.0535	0.8191
1.32mM	0.8133	0.0139	3.5918	0.0517	0.8530